



HAL
open science

Enhanced upconversion emissions in Er³⁺ doped perovskite BaTiO₃ glass-ceramics via electric-stimulated polarization technique

W. Xie, G. Bai, Y. Cai, M. Cai, Y. Tian, F. Huang, S. Xu, J. Zhang

► To cite this version:

W. Xie, G. Bai, Y. Cai, M. Cai, Y. Tian, et al.. Enhanced upconversion emissions in Er³⁺ doped perovskite BaTiO₃ glass-ceramics via electric-stimulated polarization technique. *Ceramics International*, 2019, 45 (5), pp.5392-5397. 10.1016/j.ceramint.2018.11.239 . hal-02051169v1

HAL Id: hal-02051169

<https://univ-rennes.hal.science/hal-02051169v1>

Submitted on 25 Mar 2019 (v1), last revised 26 Jun 2019 (v2)

HAL is a multi-disciplinary open access archive for the deposit and dissemination of scientific research documents, whether they are published or not. The documents may come from teaching and research institutions in France or abroad, or from public or private research centers.

L'archive ouverte pluridisciplinaire **HAL**, est destinée au dépôt et à la diffusion de documents scientifiques de niveau recherche, publiés ou non, émanant des établissements d'enseignement et de recherche français ou étrangers, des laboratoires publics ou privés.

Enhanced Upconversion Emissions in Er³⁺ doped Perovskite BaTiO₃ Glass-ceramics via Electric-Stimulated Polarization Technique

Wenqing Xie¹, Gongxun Bai¹, Yangjian Cai¹, Muzhi Cai^{1,2}, Ying Tian¹,
Feifei Huang¹, Shiqing Xu¹, and Junjie Zhang^{1,*}

¹*College of Materials Science and Engineering, China Jiliang University, Hangzhou 310018, P.R China*

²*Laboratory of Glasses and Ceramics, Institute of Chemical Science UMR CNRS 6226, University of Rennes 1, 35042 Rennes, France*

**Corresponding author: email: jjzhang@cjlu.edu.cn*

Abstract: In this work, Er³⁺ doped ferroelectric glass ceramics containing high-content BaTiO₃ nanoperovskite have been prepared successfully. Optical behaviors with structural dependence indicate that the perturbation of ligand field by tunable thermal condition in glass-ceramics is beneficial to boost upconversion efficiency, that is, the emission intensity possesses multifold improvement in both green band (²H_{11/2}, ⁴S_{3/2} → ⁴I_{15/2}) and red band (⁴F_{9/2} → ⁴I_{15/2}). And adding voltage to stimulate polarization reversal of ferroelectric domains has been investigated as a physical mode to broaden luminescence emissions in visible range. Compared with the unpolarized glass-ceramics, over 1.5 folds higher luminescence intensity can be obtained by polarizing the samples. The multiple mechanisms to achieve upconversion enhancement in ferroelectric materials will stimulate and expand the use of innovative optoelectronic devices.

Keywords: Perovskite; Thermodynamics; Upconversion; Ferroelectrics; Polarization;

1. Introduction

Within the past few years, variety of devices have focused on emerging stimulative effect by coupling two or more proprieties in a single compound, including light-emitting diodes [1], solar cell [2], non-volatile random access memories and tunable microwave [3, 4]. As a typical ferroelectric material exhibited great dielectric, piezoelectric properties and electrocaloric effect, Barium titanate (BaTiO_3) is widely used in fields of energy storage and photocoupling [5-9].

In previous reports, photo-electrical applications of perovskite BaTiO_3 particles were in great progress, mainly including nonlinear integrated photonics [10], biomedical temperature sensor [11-13], and probes for structure [14, 15]. The manufacture of low-loss BaTiO_3 -Si waveguides with propagation loss of only 6 dB/cm took the photonic integrated circuits a further step [10]. Because of the innocuity of BaTiO_3 , a number of sensors for detecting biological target temperature were underway to be fabricated [13]. Moreover, the enhancement of upconversion fluorescence was achieved in lead-free thin films and ceramics by providing electric-field stimulation [16, 17]. The relevant structural principle was revealed by means of first-principles calculations [18] and 3D imaging of ferroelectric kinetics [19]. The phenomenon can be described as a modulable electron transition mechanism of luminescent ion by perturbing structural symmetry and crystal field. Discussions regarding the conventional

methods to realize the change of crystal field around central ions have brought inevitable structural problems in disordered glassy structure, especially chemical inhomogeneities and defects [20-22]. Fortunately, the electric-stimulated polarization technique can make up for the imperfections and provide an opportunity to isolate the pure crystal-field effect from other influences in the glass-ceramics through an in-situ and reversible modulation process. In addition, residual polarization in the local environment is an indispensable part for the technique. Thanks to the typical ferroelectrics of perovskite BaTiO_3 and tunable glass components, the glass-ceramics are promising and novel electric-tunable materials to achieve controllable and reversible tuning of upconversion luminescence.

In this work, nano-sized perovskite BaTiO_3 particles are fabricated regularly in matrix glass by optimizing heat treatment processes. Crystallization kinetics of the glass-ceramics and phase structure are investigated. It is confirmed that the factors of temperature and electric field can alter crystal-field structure properly in glass-ceramics. Upconversion optical properties and the corresponding energy transfer mechanism in glass, glass-ceramics and polarized glass-ceramics are discussed by incorporating Er^{3+} ions.

2. Experiment procedures

Precursor glass samples with molar composition of $66(\text{BaO-SrO-TiO}_2)$ - 20SiO_2 - $14(\text{Al}_2\text{O}_3\text{-Na}_2\text{O})$ - $0.5\text{Er}_2\text{O}_3$ (named BTEr) were fabricated by the conventional melting method, and all the raw materials were with high purity. After weighing precisely of the starting materials, the mixed batch

was melted in an elevating furnace at 1500°C for 45 minutes. The utilization of cold-press method and primary annealing process at 600°C for 4 hours to remove the internal thermal stresses could easily obtain the precursor glass BTEr. Meanwhile, the precursor glass without rare-earth Er³⁺ named BT was melted. In the process of secondary annealing, five modes of heat treatment temperatures (810, 830, 850, 870°C) were selected. In order to precipitate crystals homogeneously, the precursor glass launched a nucleation process at 680°C for 2h with the heating rate of 2°C/min, and then a rise in temperature was carried out at the same rate. The glass-ceramics samples without Er³⁺ were named as BTT810, BTT830, BTT850 and BTT870, respectively, that doped with Er³⁺ were named as BTErT810, BTErT830, BTErT850, and BTErT870, respectively. Then, these glass-ceramics were cut into 0.2 mm thick sheets and then polished for structural, optical and ferroelectric properties testing. Adopting NETZSCH DTA 404 PC differential scanning calorimeter, the differential scanning calorimeter (DSC) curves were obtained. X-ray powder Diffract (XRD) analysis of the samples was performed with Rigaku D/max 2550 diffractometer using Cu – K α 1 radiation ($\lambda=0.154\text{nm}$). The grain orientation was measured by a transmission electron microscope (TEM, FEI Tecnai G2 F20 S-WTINE). The fluorescence spectra (400–1800nm) was measured with a computer-controlled Triax320 type spectrometer upon excitation by 980nm laser diode with the maximum power of 1 W. TDS 3012 C type Digital Phosphor Oscilloscope (100MHz, 1.25GS/S) was used to measure and

display the lifetime of the $\text{Er}^{3+}: {}^4\text{I}_{13/2}$ state. The polarization-electric field (P-E) curves were tested under the frequency of 10Hz by means of a ferroelectric testing system (Radiant Precision Premier II Technology) in a silicon oil bath to avoid electrical discharges. All the measurements were performed at room temperature.

3. Results and discussion

3.1 Thermal Kinetics

The Kissinger equation [23-25] is applied to calculate the kinetic parameters of exothermal reaction in the process of glass transition. And the specific formula is given below:

$$\ln \frac{\Psi}{T_c^2} = -\frac{E_a}{R} \frac{1}{T_c} + \ln \frac{AR}{E_a} \quad (1)$$

Where the ψ is the heating rate, E_a is apparent activation energy, R is the universal gas constant, A is pre-exponential factor, and T_c is the crystallization temperature.

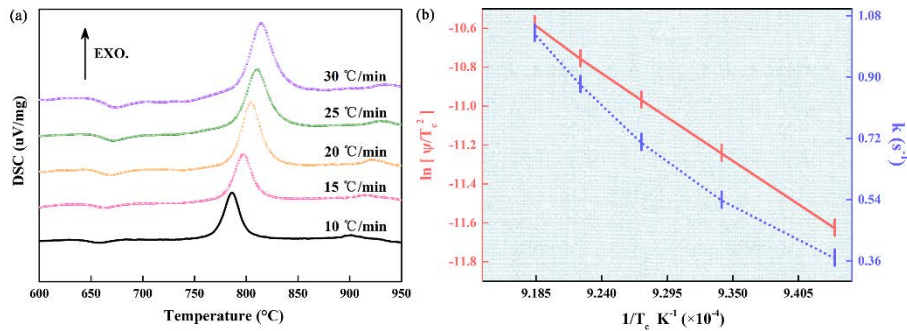


FIGURE 1. (a) DSC curves of the precursor glass at different heating rates. (b) Plot of $\ln(\psi/T_c^2)$ versus $1/T_c$ and dependence of k on $1/T_c$.

The DSC curves of glassy matrix under different heating rates of 10, 15, 20, 25, 30°C/min are recorded in FIGURE 1(a). And the linear relationship between $1/T_c$ and $\ln(\psi/T_c^2)$ launched by Formula 1 is

presented in FIGURE 1(b), yielding the kinetic parameters of E_a (kJ/mol) from the slope of the straight line and A (s^{-1}) from the intercept. The calculated activation energy $E_a=341.64\text{kJ/mol}$ and factor $A=2.51\times 10^{16}\text{s}^{-1}$ are lower than the previous reports on $(\text{Ba}_x, \text{Sr}_{1-x})\text{TiO}_3$ glass-ceramics [26, 27]. Hence, it is reasonable to believe that the BaTiO_3 nanoparticles are supposed to be fabricated in the precursor glass at a relatively low temperature as illustrated. In order to further evaluate the thermal performance, the relevant parameters listed in table 1 have been discussed. It is shown that there are two exothermic peaks of different intensities in the diagram 1(a). In silicon-based glass, a strong peak corresponding to the crystallization process of BaTiO_3 ferroelectric microcrystals is around 790°C , and a weaker peak is around 910°C . Through data analyzing, the invariant ΔT (about 154°C) points out a high thermal stability of the precursor glass. Besides, the calculation of fragility [28] ($m=E_a/RT_g$) indicates a dense and stable glass network structure.

Table 1. Heating rate, crystallization temperatures, crystallization temperature, crystallization peak temperature, stabilization temperature, fragility obtained from activation energy, activation energy, reaction rate and crystal growth dimension of precursor glass.

$\psi(^{\circ}\text{C}/\text{min})$	$T_g(^{\circ}\text{C})$	$T_x(^{\circ}\text{C})$	$T_c(^{\circ}\text{C})$	ΔT	$E_a(\text{kJ}/\text{mol})$	A	m	k
10	619.2	768.4	786.7	149.3			46.05	0.37
15	621.4	778.2	797.5	156.8			52.80	0.54
20	627.3	784.0	805.2	156.7	341.64	2.51×10^{16}	52.41	0.71
25	633.4	786.7	811.2	153.4			52.23	0.88
30	636.3	790.2	816.0	154.0			52.00	1.03

Arrhenius theory [26], $k=Ae^{-E_a/RT}$, is an important equation to compute the rate of crystallization, and the relationship between k and $1/T_c$ is plotted in FIGURE 1(b). It is illustrated that the crystallization rate k is increased accompanying by the crystallization temperature T_c , which implies that manifold effective collision particles activate the crystallization process. In terms of chemical composition, the increased non-bridged oxygen and reduced activation energy are presented as the addition of alkali metal carbonate Na_2CO_3 . These results stimulate the increase of crystallization.

3.2 Phase analysis

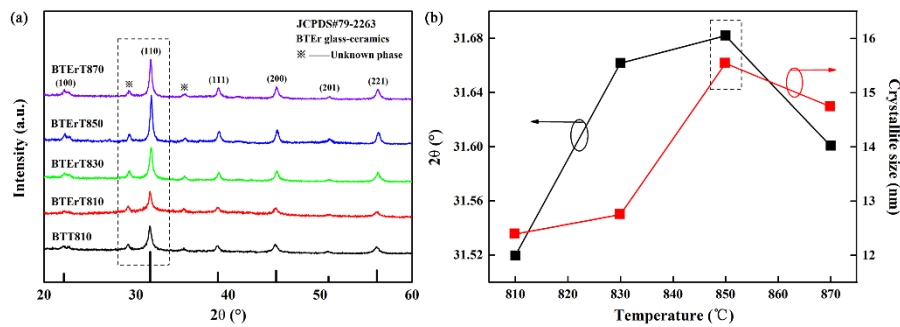


FIGURE 2. (a) The XRD patterns of the glass ceramics. (b) The variation trends of peak position of (110) surface and the grain size of nanoparticles.

The X-ray diffractometer (XRD) patterns of glass ceramics BTT810, BTErT810, BTErT830, BTErT850, and BTErT870 are depicted in FIGURE 2(a). It can be clearly seen that all peaks from 20° to 60° correspond well to the XRD pattern of cubic $BaTiO_3$ phase (JCPDS card No.79-2263 with space group $Pm-3m$ and the lattice constants of $a=b=c=4.006\text{\AA}$, $z=1$), except for two unknown tiny diffraction peaks located at 29.26° and 35.69° . Contrasting monitoring data, the characteristic peaks gradually shift towards larger angle with the

increment of crystallization temperature, and the tendency is established in FIGURE 2(b). It is revealed that the reduced crystallite volume provides the possibility of Er^{3+} ions percolating into the BaTiO_3 structure. Referring to previous report came from Prof. Hao [17], the conclusion of Er^{3+} replaced Ti^{4+} in BaTiO_3 glass ceramics can be obtained by analogy, as displayed in model S1 in FIGURE 3(a). Besides, the embed model S2 demonstrates the substitution of Er^{3+} for Ba^{2+} , due to the atomic size of Er^{3+} (1.03Å) is smaller than Ba^{2+} (1.75Å). In addition, model S3 contains both of the above two cases.

The crystallite size can be calculated by using Scherer formula [29], as follows:

$$d = \frac{K\lambda}{\beta \cos \theta} \quad (2)$$

where K is the shape factor (0.94), λ is the wavelength of Cu K_α line (1.54Å) and β is the full width at half maximum. The grain size obtained at different heat treatment temperatures is plotted in FIGURE 2(b). By differing temperature, the same positive trends of the peak position and grain size are obtained at 850°C. But continuing to grow up the temperature, a weakened result will be found. In addition, this anomaly can also be observed in the subsequent spectroscopic analysis.

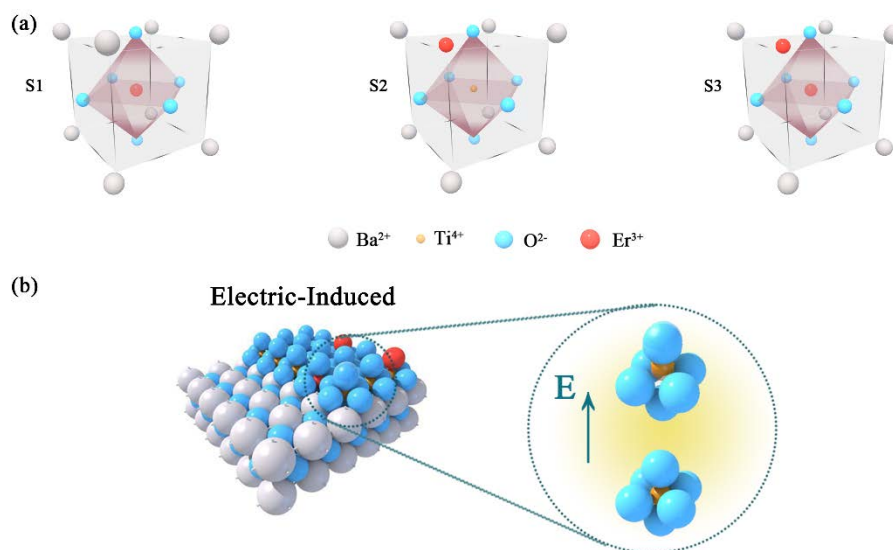


FIGURE 3. (a) 3D substitution models of BaTiO₃ unit cell. (b) Local atomic distribution of BaTiO₃ perovskite particles and the offsets of Ti-O atoms after polarizing.

3.3 Emission characteristic effected by rmdynamics

As a typical rare-earth luminescent ion, the emission intensity of Er³⁺ is affected by the crystal symmetry of host materials whether to emit upconversion visible or downconversion near infrared photoluminescence (PL) [22, 30]. The PL spectrums of Er³⁺ incorporated into BaTiO₃ ferroelectric glass-ceramics in the visible region are measured and depicted in FIGURE 4. It is presented that there are three main emission peaks around 534nm, 557nm and 665nm, corresponding to ${}^2H_{11/2} \rightarrow {}^4I_{15/2}$, ${}^4S_{3/2} \rightarrow {}^4I_{15/2}$, and ${}^4F_{9/2} \rightarrow {}^4I_{15/2}$, respectively. Obviously, the upconversion luminescence is enhanced by secondary annealing process, and the maximum multiples located in main green band (557nm) can reach up to 10.05 folds. Meanwhile, the PL intensity ratio between glass ceramics (heat-treated at 850°C) and the precursor glass is up to 17.96 at the red band. But the emission intensity begins to fade down along with the

continuous heating-up to 870°C. This phenomenon is related to the concentration quenching effect since more Er^{3+} ions incorporates into the BaTiO_3 crystallites with the increasing of crystallization temperature [31].

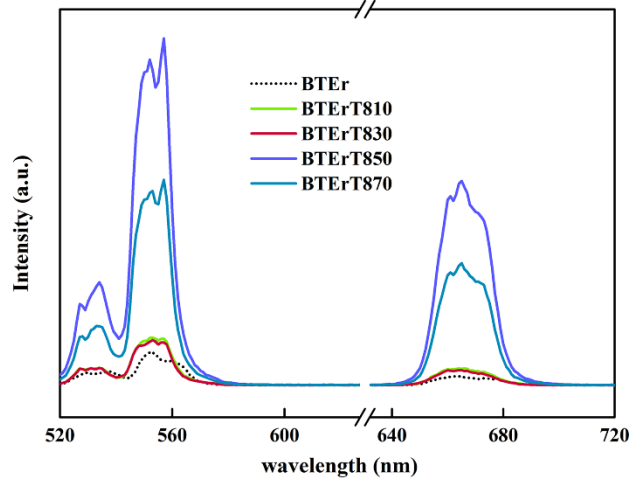


FIGURE 4. Upconversion emission spectra of Er^{3+} .

A Hamiltonian [32, 33] is introduced to describe the energy transition of the entire system. The formula is as follows:

$$H = H_0 + V_{\text{crystal-field}} + V_{EM} + V_{\text{ion-ion}} \quad (3)$$

Where H_0 is the role of electron and spherical symmetry ion core, $V_{\text{crystal-field}}$ is the effect of lattice field, V_{EM} is an interaction between ions and electromagnetic fields, $V_{\text{ion-ion}}$ is the interaction of two Er^{3+} . How the internal electrons of Er ions affected by crystal field can be further understood from the perspective of quantum mechanics. In the precursor glass, the change of crystal field has little impact on the oninner ground state electrons due to the 4f-4f electrons of Er^{3+} are shielded by the outer electron, and only can be regarded as a small disturbance [34]. But in FIGURE 4, the obvious stark split peaks indicate that the weak change around the Er^{3+} after crystallizing drives the crystal field asymmetrical so

as to increase the $V_{\text{crystal-field}}$. Since Er^{3+} can replace Ti^{4+} and occupy the center of the octahedron surrounded by oxygen ions, the deviated Er^{3+} caused by unbalanced electrovalence changes the H_0 . Notably, the increase of H opens a reliable gate to explain the unusual emission enhancement phenomenon.

3.4 Emission characteristic effected by electric field

Further enhanced emission of the green band has been achieved, as reflected in a series of exploratory experiments in FIGURE 5, by applying a high bias voltage (160V) to the glass-ceramics subtlety. It is obvious that, the glass-ceramics obtained at 850°C get the best up-conversion luminescence.

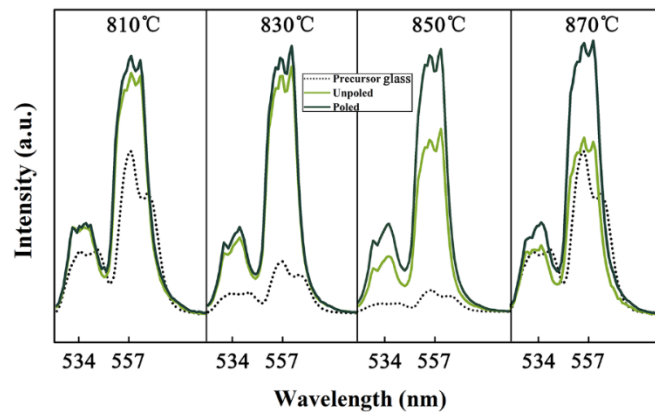


FIGURE 5. Fluorescence emission spectra of different glass-ceramics at the green band.

Optical tests on the glass-ceramics sample BTErT850 (fabricated at 850°C) are carried out in depth, referring to previous reports [9, 35]. The luminescent properties of BTErT850 samples are measured and depicted in FIGURE 6(a) and (b). In addition to the heightened multiples mentioned above, it is observed in FIGURE 6(a) that the ${}^2\text{H}_{11/2}$, ${}^4\text{S}_{3/2} \rightarrow {}^4\text{I}_{15/2}$ and

${}^4F_{9/2} \rightarrow {}^4I_{15/2}$ emissions of Er^{3+} are almost enhanced about 1.5 times by applying a voltage of 160V to the BTErT850 for polarization. By contrast, the unpoled BTErT850 and poled BTErT850 both showed a weaker emission than the precursor glass in the near-infrared band, resulting in a gap of about 2.5 times.

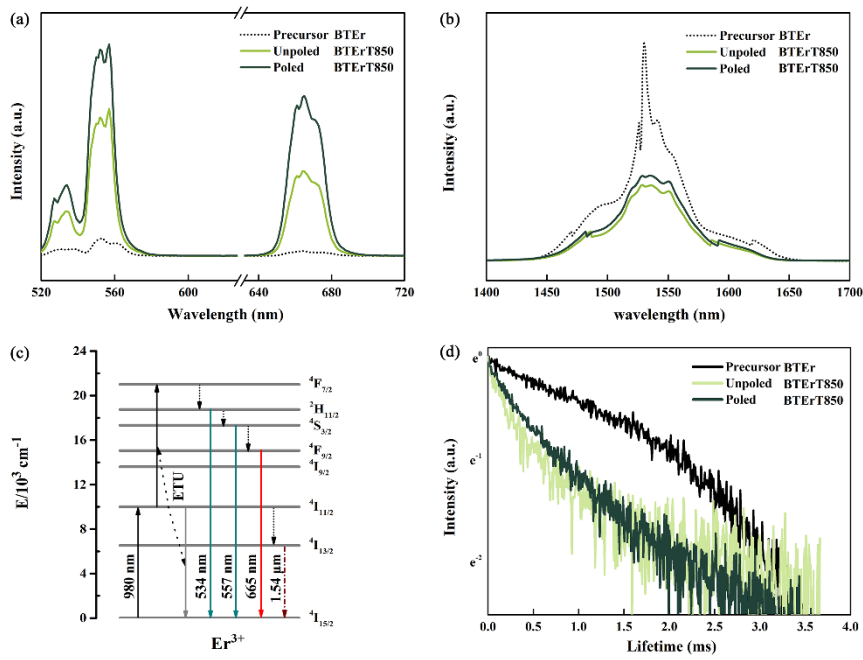


FIGURE 6. (a) Upconversion emission spectra of Er^{3+} . (b) Near-infrared emission spectra of Er^{3+} (1.54 μm). (c) Energy transfer mechanism of Er^{3+} . (d) Measured near-infrared decay curves.

The decreased near-infrared (1.54 μm) emission of Er^{3+} is attributed to enhance upconversion emission of Er^{3+} . To verify this point, energy level transition dynamic is provided in FIGURE 6(c). Upconversion luminescence of RE ions is the result of a dynamic process or a combination of several processes. The 980nm laser excites the electrons of ${}^4I_{15/2} \rightarrow {}^4I_{11/2}$ of Er^{3+} with a ground state absorption (GSA), which acts as a two-photon process. On account of the increasing particles at the ${}^4I_{11/2}$

level with the changing in glass conditions (precipitating crystallites and electric-field polarization), the excitation state absorption (ESA) and energy transfer up-conversion processes (ETU) are enhanced appreciably. In consequence of the increased number of Er^{3+} transitioning from the $^4\text{I}_{11/2}$ level to $^4\text{F}_{7/2}$ and rapidly relaxed to $^4\text{S}_{3/2}$ and $^4\text{F}_{9/2}$ through the non-radiative transition, the green light (557nm) and the red light (665nm) are excited to a greater extent. Comparatively, the radiation transition of $^4\text{I}_{11/2} \rightarrow ^4\text{I}_{13/2}$ is noticeably attenuated corresponding to the weakness of luminescence at 1.54 μm . The time-resolved near-infrared fluorescence spectra were conclusively showed in FIGURE 6(d). According to the fitting calculation, the fluorescence lifetime of the precursor glass is 2.07ms. Conversely, much shorter lifetimes are present to the glass-ceramic samples of unpoled BTErT850 (0.55ms) and poled BTErT850 (0.79ms). The polarization-dependent time-resolved luminescent behaviors are in good agreement with the near-infrared emission spectra of Er^{3+} at 1.54 μm . The data consistency verifies that the effect of electric-induced polarization allows the luminous efficiency of Er^{3+} to be enhanced at both up-conversion and down-conversion luminescence.

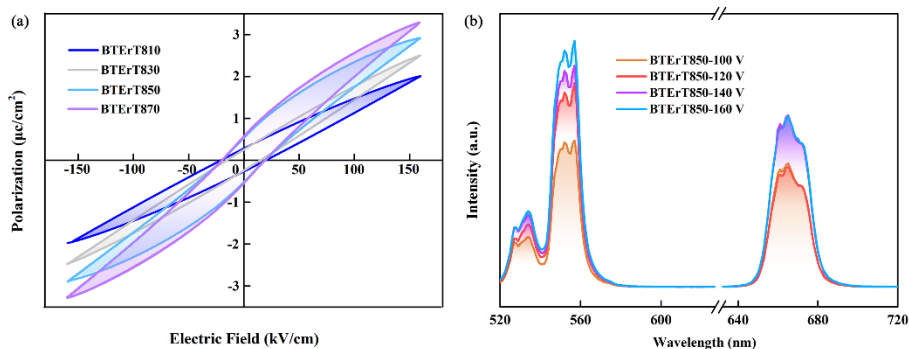


FIGURE 7. (a) Polarization hysteresis loop of samples obtained at different treatment temperatures. (b) Fluorescence emission pattern of sample BTErT850 under different electric fields. For purpose of verifying the positive correlation between remanent polarization and photoluminescence, the typical E-P loops at different dc bias voltage and the PL spectrum of BTErT850 samples poled by increased voltage are demonstrated in the FIGURE 7(a) and 7(b). It indicates that the original disordered ferroelectric domain turns to a relatively uniform orientation exactly as the applied electric field, which leads to be modified of the ligand field around rare-earth ions. More specially, under the modulation of the electric field, the relative displacement of Ti-O is altered slightly. That is, Ti^{4+} moves toward the electric field and O^{2-} is in the opposite direction, referring to FIGURE 3(b). Thereby the incremental emission intensity of the polarized glass-ceramics is reflected positively as illustrated in FIGURE 7(b).

4. Conclusions

In summary, Er^{3+} doped ferroelectric glass ceramics containing BaTiO_3 nanoperovskite are successfully synthesized. The upconversion emission intensity in the visible is obtained to acquire significant enhancement after engaging in a secondary annealing progress, and the maximum intensity increment of green light (${}^2\text{H}_{11/2}$, ${}^4\text{S}_{3/2} \rightarrow {}^4\text{I}_{15/2}$) is about 10.05 folds while the red light (${}^4\text{F}_{9/2} \rightarrow {}^4\text{I}_{15/2}$) is 17.96 folds. Furthermore, the fluorescence intensity of the polarized glass-ceramics suffered from a 160 V dc bias voltage is able to improve almost 1.5 folds. The results performs that the

present ferroelectric glass-ceramic is promising to develop a sensitive and efficient optoelectronic device in the future applications.

Acknowledgments. This research was financially supported by Chinese National Natural Science Foundation (No 61705214, 61605192 and 61775205) and Zhejiang Provincial Natural Science Foundation of China (No LD18F050001).

References

- [1] L. Meng, E.P. Yao, Z. Hong, H. Chen, P. Sun, Z. Yang, G. Li, Y. Yang, Pure Formamidinium-Based Perovskite Light-Emitting Diodes with High Efficiency and Low Driving Voltage, *Adv. Mater.* 29 (2017).
- [2] H. Chen, F. Ye, W. Tang, J. He, M. Yin, Y. Wang, F. Xie, E. Bi, X. Yang, M. Gratzel, L. Han, A solvent- and vacuum-free route to large-area perovskite films for efficient solar modules, *Nature*. 550 (2017) 92-95.
- [3] A. Kumar, S.G. Manavalan, Characterization of barium strontium titanate thin films for tunable microwave and DRAM applications, *Surf. Coat. Technol.* 198 (2005) 406-413.
- [4] H. Yu, C.-C. Chung, N. Shewmon, S. Ho, J.H. Carpenter, R. Larrabee, T. Sun, J.L. Jones, H. Ade, B.T. O'Connor, F. So, Flexible Inorganic Ferroelectric Thin Films for Nonvolatile Memory Devices, *Adv. Funct. Mater.* 27 (2017) 1700461.
- [5] S. Chihaoui, L. Seveyrat, V. Perrin, I. Kallel, L. Lebrun, H. Khemakhem, Structural evolution and electrical characteristics of Sn-doped $\text{Ba}_{0.8}\text{Sr}_{0.2}\text{TiO}_3$ ceramics, *Ceram Int.* 43 (2017) 427-432.
- [6] Q. Feng, X.y. Liu, G.h. Chen, X. Liu, C.g. Yuan, Z.x. Jiang, C.g. Zhou, Dielectric, ferroelectric and energy storage properties of $(1-x)\text{Bi}_{0.47}\text{Na}_{0.47}\text{Ba}_{0.06}\text{TiO}_3-x\text{BaZrO}_3$ glass ceramics, *J. Mater. Sci.: Mater. Electron.* 27 (2016) 6282-6291.
- [7] H. Sun, X. Wu, D.F. Peng, K.W. Kwok, Room-Temperature Large and Reversible Modulation of Photoluminescence by in Situ Electric Field in Ergodic Relaxor Ferroelectrics, *ACS Appl. Mater. Interfaces.* 9 (2017) 34042-34049.
- [8] Z. Wu, Y. Zhang, G. Bai, W. Tang, J. Gao, J. Hao, Effect of biaxial strain induced by piezoelectric PMN-PT on the upconversion photoluminescence of $\text{BaTiO}_3:\text{Yb}/\text{Er}$ thin films, *Opt Express.* 22 (2014) 29014-29019.
- [9] G. Bai, Y. Zhang, J. Hao, Tuning of near-infrared luminescence of $\text{SrTiO}_3:\text{Ni}^{2+}$ thin films grown on piezoelectric PMN-PT via strain engineering, *Sci. Rep.* 4 (2014) 5724.
- [10] F. Eltes, D. Caimi, F. Fallegger, M. Sousa, E. O'Connor, M.D. Rossell, B. Offrein, J. Fompeyrine, S. Abel, Low-Loss $\text{BaTiO}_3\text{-Si}$ Waveguides for Nonlinear Integrated Photonics, *ACS Photonics.* 3 (2016) 1698-1703.
- [11] Y. Zhang, X. Chai, J. Li, X. Wang, Y. Li, X. Yao, Enhanced up-conversion luminescence and excellent temperature sensing properties in Yb^{3+} sensitized Er^{3+} -doped $\text{Bi}_3\text{Ti}_{1.5}\text{W}_{0.5}\text{O}_9$ multifunctional ferroelectric ceramics, *J. Alloys. Compd.* 735 (2018) 473-479.
- [12] P. Du, L.H. Luo, J.S. Yu, Low-temperature thermometry based on upconversion emission of Ho/Yb-codoped $\text{Ba}_{0.77}\text{Ca}_{0.23}\text{TiO}_3$ ceramics, *J. Alloys Compd.* 632 (2015) 73-77.
- [13] M. Jia, G. Liu, Z. Sun, Z. Fu, W. Xu, Investigation on Two Forms of Temperature-Sensing Parameters for Fluorescence Intensity Ratio Thermometry Based on Thermal Coupled Theory, *Inorg. Chem.* 57 (2018) 1213-1219.
- [14] H. Zhou, G. Wu, N. Qin, D. Bao, H. Wang, Improved Electrical Properties and Strong Red Emission of Pr^{3+} -Doped $x\text{K}_{0.5}\text{Bi}_{0.5}\text{TiO}_3-(1-x)\text{Na}_{0.5}\text{Bi}_{0.5}\text{TiO}_3$ Lead-Free Ferroelectric Thin Films, *J. Am. Ceram. Soc.* 95 (2012) 483-486.
- [15] W. Huang, S. He, A. Hao, N. Qin, M. Ismail, J. Wu, D. Bao, Structural phase transition, electrical and photoluminescent properties of Pr^{3+} -doped $(1-x)\text{Na}_{0.5}\text{Bi}_{0.5}\text{TiO}_3-x\text{SrTiO}_3$ lead-free ferroelectric thin films, *J. Eur. Ceram. Soc.* 38 (2018) 2328-2334.
- [16] H. Zou, D. Peng, G. Wu, X. Wang, D. Bao, J. Li, Y. Li, X. Yao, Polarization-induced enhancement of photoluminescence in Pr^{3+} doped ferroelectric diphase $\text{BaTiO}_3\text{-CaTiO}_3$ ceramics, *J. Appl. Phys.* 114 (2013) 073103.

- [17] J. Hao, Y. Zhang, X. Wei, Electric-induced enhancement and modulation of upconversion photoluminescence in epitaxial BaTiO₃:Yb/Er thin films, *Angew. Chem.* 50 (2011) 6876-6880.
- [18] Y.S. Oh, X. Luo, F.T. Huang, Y. Wang, S.W. Cheong, Experimental demonstration of hybrid improper ferroelectricity and the presence of abundant charged walls in (Ca,Sr)₃Ti₂O₇ crystals, *Nat. Mater.* 14 (2015) 407-413.
- [19] M. Ayoub, H. Futterlieb, J. Imbrock, C. Denz, 3D Imaging of Ferroelectric Kinetics during Electrically Driven Switching, *Adv. Mater.* 29 (2016).
- [20] Y. Zhang, W. Jie, P. Chen, W. Liu, J. Hao, Ferroelectric and Piezoelectric Effects on the Optical Process in Advanced Materials and Devices, *Adv. Mater.* (2018) e1707007.
- [21] Q. Liu, Y. Tian, W. Tang, F. Huang, X. Jing, J. Zhang, S. Xu, Broadening and enhancing 2.7 μm emission spectra in Er/Ho co-doped oxyfluoride germanosilicate glass ceramics by imparting multiple local structures to rare earth ions, *Photon. Res.* 6 (2018) 339.
- [22] T.-C. Huang, W.-F. Hsieh, Er-Yb Codoped Ferroelectrics for Controlling Visible Upconversion Emissions, *J. Fluoresc.* 19 (2008) 511-516.
- [23] F.-G. Wei, M. Enomoto, K. Tsuzaki, Applicability of the Kissinger's formula and comparison with the McNabb-Foster model in simulation of thermal desorption spectrum, *Comput. Mater. Sci.* 51 (2012) 322-330.
- [24] D. Souri, H. Zaliani, E. Mirdawoodi, M. Zendezhaban, Thermal stability of Sb-V₂O₅-TeO₂ semiconducting oxide glasses using thermal analysis, *Meas.* 82 (2016) 19-25.
- [25] B. Li, S. Wang, Y. Fang, Effect of Cr₂O₃ addition on crystallization, microstructure and properties of Li₂O-Al₂O₃-SiO₂ glass-ceramics, *J. Alloys Compd.* 693 (2017) 9-15.
- [26] A.K. Yadav, C.R. Gautam, P. Singh, Crystallization and dielectric properties of Fe₂O₃ doped barium strontium titanate borosilicate glass, *Rsc. Adv.* 5 (2015) 2819-2826.
- [27] A.K. Yadav, C. Gautam, P. Singh, Crystallization Kinematics and Dielectric Behavior of (Ba,Sr)TiO₃ Borosilicate Glass Ceramics, *New J. Glass Ceram.* 02 (2012) 126-131.
- [28] D. Souri, Physical and thermal characterization and glass stability criteria of amorphous silver-vanadate-tellurate system at different heating rates: Inducing critical Ag₂O/V₂O₅ ratio, *J. Non-Cryst. Solids.* 475 (2017) 136-143.
- [29] C.R. Gautam, A.K. Yadav, P. Singh, Synthesis, crystallisation and microstructural study of perovskite (Ba,Sr)TiO₃ borosilicate glass ceramic doped with La₂O₃, *Mater. Res. Innovations.* 17 (2013) 148-153.
- [30] S. Heer, K. Koempe, H U. Guedel, et al. Highly Efficient Multicolor Upconversion Emission in Transparent Colloids of Lanthanide-Doped NaYF₄ Nanocrystals. *Adv. Mater.* 36 (2010) 2102-2105.
- [31] P. Riello, S. Bucella, L. Zamengo, U. Anselmi-Tamburini, R. Francini, S. Pietrantoni, Z.A. Munir, Erbium-doped LAS glass ceramics prepared by spark plasma sintering (SPS), *J. Eur. Ceram. Soc.* 26 (2006) 3301-3306.
- [32] K.A. Müller, H. Burkard, SrTiO₃: An intrinsic quantum paraelectric below 4 K, *Phys. Rev. B.* 19 (1979) 3593-3602.
- [33] N.C. Chang, J.B. Gruber, R.P. Leavitt, C.A. Morrison, Optical spectra, energy levels, and crystal - field analysis of tripositive rare earth ions in Y₂O₃. I. Kramers ions in C₂ sites, *J. Chem. Phys.* 76 (1982) 3877-3889.
- [34] S.-Y. Kuo, C.-S. Chen, T.-Y. Tseng, S.C. Chang, W.-F. Hsieh, Dependence of luminescence efficiency on dopant concentration and sintering temperature in the erbium-doped Ba_{0.7}Sr_{0.3}TiO₃ thin films, *J. Appl. Phys.* 92 (2002) 1868-1872.
- [35] G.x. Bai, W.j. Jie, Z.b. Yang, J.h. Hao, Temperature dependence of broadband near-infrared luminescence from Ni²⁺-doped Ba_{0.5}Sr_{0.5}TiO₃, *J. Appl. Phys.* 118 (2015) 183110.